Asteroid Impact Risk Changes Due To Disruption By A Deflection Mission

Clemens M. Rumpf[1,2], Lorien F. Wheeler[1], Javier Roa[3], Davide Farnocchia[3], Jessie L. Dotson[1]

[1]NASA Ames Research Center, Moffett Field, CA 94035, USA
[2]STC, NASA Research Park, Moffett Field, CA 94035, USA
[3]Jet Propulsion Laboratory, California Institute of Technology, 4800 Oak Grove Drive, Pasadena, CA 91109, USA

Key Points:

- For this Apophis scenario, weak disruption causes $> 3\times$ impact risk increase.
- Potential for disruption should be a main consideration in the mitigation mission design and decision process.
- Identifies impact risk dependency on disrupted asteroid size. A threshold exists under which risk decreases in a disruption event.

Corresponding author: Clemens M. Rumpf, drcrumpf@gmail.com

Abstract

This study examines the impact risk consequences due to asteroid disruption by a deflection mission. We use an Apophis-like scenario with a Nuclear Explosive Device (NED) deflection mission in our case studies. A Monte Carlo framework samples asteroid physical properties from probabilistic distributions based on the current knowledge of Apophis, and samples orbital states from an archival orbit solution reflecting Apophis' 2.7 % peak impact probability. Asteroid disruption is modelled at deflection time and the fragments are propagated forward to calculate if and where they impact the Earth. NASA's Probabilistic Asteroid Impact Risk (PAIR) model estimates the impact damage in terms of affected population, and the overall scenario impact risk is calculated. Multiple case studies are explored to generate comparative data for scenarios where the asteroid is not altered, is always disrupted, or is conditionally disrupted with deflection impulse. The analysis shows that disruption increases impact risk for this Apophis scenario significantly. Even though deflection missions may cause disruption, a sufficiently strong deflection mission can be effective as risk decreases from its post-disruption peak with increasing deflection strength. Results also point to the dependence of risk changes on physical properties. Objects with a fraction of Apophis' mass will result in less risk when disrupted. We recommend that disruption analysis should be a critical factor in future asteroid mitigation considerations and suggest future research avenues of interest to mission design as well as planetary sciences.

Plain Language Summary

A deflection mission can be launched to change the trajectory of an asteroid threatening to impact the Earth. However, such a deflection mission might also disrupt the asteroid into several fragments. Disruption opens up the possibility to have multiple fragments impacting the Earth instead of a single larger asteroid. This study is motivated by the question of what would be worse: One asteroid that impacts the Earth as a single body or multiple smaller fragments. To assess the severity of an impact scenario on the Earth, we use tools to calculate the number of affected population by an impact and express this as impact risk. We find that disruption can significantly aggravate the risk posed by a threatening asteroid. We also find that deflection missions are still an effective means to mitigate the threat of an impacting asteroid. However, such deflection missions should take into account the possibility of disruption and may need to be more powerful than previously anticipated. Finally, we find that the answer to the question of whether disruption increases impact risk depends on the size (and other parameters) of the asteroid. For small asteroids, the impact risk appears to decrease with disruption.

1 Introduction

The asteroid impact hazard poses an existential threat to civilisations on the Earth (Chapman & Morrison, 1994). There is ample archaeological evidence of the destructive potential of asteroid impacts. Dinosaurs went extinct after a large impact (Alvarez et al., 1980), and numerous impact craters are present on the Earth, Moon and other planets (Hergarten & Kenkmann, 2015). In 1908, an airburst event over Siberia's Tunguska region flattened a forested area comparable in size to that of a large metropolitan region such as London (Chyba et al., 1993; Robertson & Mathias, 2019). More recently, in 2013, a smaller airburst injured over 1500 people in Chelyabinsk, Russia (Popova et al., 2013).

The possibility of threat mitigation by human intervention makes the asteroid impact hazard stand out from other natural disasters. To avert a potential impact threat, a deflection or disruption mission is needed. In a deflection mission, the spacecraft intercepts the asteroid and attempts to change its trajectory such that the asteroid either

misses the Earth or impacts in a new location where minimal damage is expected. Such deflection could be accomplished either with slow push/pull methods, such as gravity tractors, or impulsive techniques, such as kinetic impactors (KI) or stand-off nuclear detonation (Shapiro et al., 2010). Impulsive techniques provide greater deflection capabilities over shorter periods of time. However, an impulsive deflection mission might also (intentionally or unintentionally) disrupt the target asteroid, thereby creating multiple fragments that can hit the Earth independently. This situation may arise because the majority of asteroids tend to be loosely bound *rubble piles* that are easily disrupted (Walsh et al., 2008; Pravec et al., 2010; Sánchez & Scheeres, 2014). The question addressed in this research article is whether a deflection mission that disrupts the asteroid could worsen the impact threat because multiple smaller impacts in several locations are created. Or, does disruption decrease impact risk because smaller impacts are less severe than a single large one?

This work builds on ongoing efforts to characterize the risk to human life of asteroid impacts. Previous works have focused on estimating the ensamble risk posed by the general asteroid population, which could naturally impact the Earth at various intervals (Mathias et al., 2017; Reinhardt et al., 2016; Rumpf et al., 2017; Stokes et al., 2017). Assessing how a specific deflection mission would alter the risk situation on the ground became the next logical extension to previous threat assessment tools (Rumpf et al., 2020). With the capability of asteroid deflection on the table, our research turned to the question of how deflection-induced disruption of the asteroid would alter the risk situation. Just as a deflection mission can alter the risk situation on the ground in unexpected ways, disruption could have the potential to produce unintentional and grave consequences which might worsen the risk situation by human intervention.

In this study, we focus on the impulsive nuclear explosive device (NED) deflection technique. However, the concerns associated with disruption apply to kinetic impactors—another prominent deflection technique (Cheng et al., 2018)—as well. We selected the NED approach due to its easy scalability in terms of deflection impulse, which provides flexibility for the present study.

We applied detailed orbital propagation models that track each fragment as a result of disruption, predict their impact location on the Earth, and estimate the resulting damage in terms of affected population. Previous work by Sanchez et al. (2010) has looked at changing damage potentials of asteroid impacts due to disruption. Their work relied on indirect damage analysis where expected tsunami potential and blast radii estimates were used as proxy for damage severity without knowledge of impact locations. Sanchez et al. (2010) asserted reduced, yet still significant, damage potential after disruption for an Apophis-like scenario. In our analysis, we provide evidence that disruption might in fact significantly increase the risk after disruption. Such information is essential for mission designers and public decision makers. This analysis approach could also be used to establish science target priorities for in-situ asteroid research to constrain physical properties that drive the disruption potential and subsequent risk changes. Equally, the work could be used to establish minimum NED yield strength to sufficiently disrupt an asteroid such that fragments are small and dispersed wide enough to miss the Earth or cause minimal damage.

2 Method

The simulation framework mirrors the general setup described in more detail in Rumpf et al. (2020). A two-layered Monte Carlo (MC) framework was used to sample the multi-dimensional distribution space that describes the physical and orbital characteristics of the Apophis-like scenario. In the first layer, a set of samples was drawn from the asteroids physical property distributions (Figure 1). The set of physical properties provided a complete representation of the asteroid in this MC run. In the second layer, random

samples were drawn from the orbit solution (see section 2.1). The trajectory of each orbit sample was propagated to deflection (see section 2.3) where disruption of the asteroid may occur depending on the criteria laid out in sections 2.4 and 2.5. Only those orbit samples that were on a natural impact trajectory with the Earth were deflected/disrupted . The underlying rationale being that a deflection mission would improve asteroid ephemeris quality sufficiently through relative navigation during final approach to confirm whether the asteroid would impact the Earth. Only an asteroid on an impacting trajectory would be targeted by the deflection mission. As such, in this analysis, the simulated deflection action only moved samples off of the Earth but never onto it. Finally, the fragments were propagated forward in time to their impact location on the Earth. For each impact case, the Probabilistic Asteroid Impact Risk (PAIR) tool (Mathias et al., 2017) was used to model the impact damage and estimate the number of people affected. The results of each MC run were recorded, and the risk outcome (see section 2.6) of the entire scenario was calculated.

PAIR is a fast running impact risk assessment tool. It models the impacting object's atmospheric entry and corresponding process of catastrophic fragmentation (L. F. Wheeler et al., 2017). The energy released during an atmospheric airburst or ground impact is the basis to estimate major damage mechanisms such as local blast wave (Aftosmis et al., 2019) and thermal radiation, together with far ranging tsunamis and global effects. The local population that is within reach of the damage mechanisms is counted and contributes to the affected population, or damage, of that impact. The proportion of the population that is counted towards affected population decreases with lessening impact effect severity (Mathias et al., 2017). In this study, all damage effects, except for global effects, were taken into account. It is possible that an Apophis class impact could have long-term, global consequences such as dust deposition in the atmosphere. However, here we only consider short-term consequences which are not expected to occur in the present impactor size regime (Covey et al., 1994). PAIR estimates the spatial extend of the damage mechanisms around the impact site and records the number of population in that region that would either be fatally or seriously injured (Stokes et al., 2017). In this article, we call the injured or killed population *affected population* and this is a key metric used to calculate risk.

The baseline impact scenario, in which no disruption or deflection was considered, used 2000 impact points and 5000 physical property sets (10 million unique MC runs, with each asteroid property case impacting at each location). Each case study to assess the effect of deflection and disruption used 3000 orbit samples and 5000 physical property sets.

If disruption occurred, up to 20 fragments were generated and propagated individually to impact, for a total of between 15 million (no disruption) and 300 million (asteroid disrupts into 20 fragments in all cases) unique MC runs. A value of 20 fragments was chosen as a compromise between the ideal condition of allowing for a large number of fragments and maintaining computational tractability. A choice of 20 fragments as the upper limit is considered suitable because this study explores the effect of weak disruption on impact risk. Weak disruption means that the excess energy delivered during the deflection attempt is similar to the amount needed for asteroid disruption. This condition was chosen to produce scenarios that rely on the same deflection action while comparing outcomes in which disruption did and did not occur. In general, the excess energy delivered during deflection drives fragment sizing and count (Fujiwara et al., 1977). A low energy, weak disruption will yield fewer, larger fragments, while a very energetic deflection will produce more, smaller fragments. Since this study works with low-energy disruption, an upper limit of 20 fragments should be adequate for analysis. Nevertheless, it is possible that the selection of this specific upper limit fragment count introduced a bias in the results of this study. The topic of bias due to fragment count setting should be investigated in the future and was not treated as part of this analysis.

Epoch TDB	2004-11-26.0
Eccentricity	0.1912472 ± 0.0000236
Perihelion distance	0.7456921 ± 0.0000161 au
Time of perihelion TDB	2004-09-28.64950 ± 0.00488 d
Longitude of node	204.56986° ± 0.00385°
Argument of perihelion	126.19869° ± 0.00651°
Inclination	3.333657° ± 0.000387°

Table 1. JPL solution 15 for Apophis with 1-σ formal uncertainties. The osculating heliocentric orbital elements are in the IAU76 ecliptic frame (Seidelmann, 1977).

The NASA HECC[1] Pleiades computing cluster was used to run the simulations. Each case study typically utilized about 2000 CPUs and required about 3 hrs of run-time, excluding post-processing of results.

2.1 Orbit solution

Apophis was discovered by R.A. Tucker, D.J. Tholen, and F. Bernardi at Kitt Peak, Arizona on 2004 June 19 (Minor Planet Supplement 109613)[2]. The initial two nights of observations had significant astrometric reduction problems and, in the following days, telescope scheduling issues, bad weather, and lunar interference prevented the collection of additional observations. In December 2004, Apophis was serendipitously reobserved by G.J. Garradd at Siding Springs, Australia (MPEC 2004-Y25).[3] At that point it became obvious that Apophis was going to make a deep close approach to Earth in April 2029 with significant chances of an impact. As new astrometric measurements were collected, the impact probability increased, reaching a peak of 2.7%, until precovery observations from March 2004 reported by the Spacewatch survey (MPEC 2004-Y70)[4] ruled out the possible impact in 2029 (Chesley, 2006).

Since 2004, Apophis has been regularly tracked and an extensive dataset of optical and radar astrometry tightly constrains its orbit. While Apophis remains a consideration in terms of impact hazard for the second part of the century (Vokrouhlický et al., 2015), the circumstances of the 2029 close encounter can be accurately predicted and the miss distance will be about 38,000 km (Brozović et al., 2018)

For the purpose of this paper, we use JPL solution 15, which is shown in Table 1. This early solution is based on a data arc from 19 June 2004 to 27 December 2004 and corresponds to the peak impact probability for 2029.

2.2 Physical Properties

The physical properties were generated by an inference network, which probabilistically generated properties based on the properties of the near-Earth asteroid population, likely relationships between the properties, and available characterization measurements of Apophis. The output of this network consists of 5,000 sets of plausibly linked physical parameters representing the state of our current knowledge about Apophis.

[1] `https://www.nas.nasa.gov/hecc/`
[2] `https://www.minorplanetcenter.net/iau/ECS/MPCArchive/2004/MPS_20040627.pdf`
[3] `https://www.minorplanetcenter.org/mpec/K04/K04Y25.html`
[4] `https://www.minorplanetcenter.org/mpec/K04/K04Y70.html`

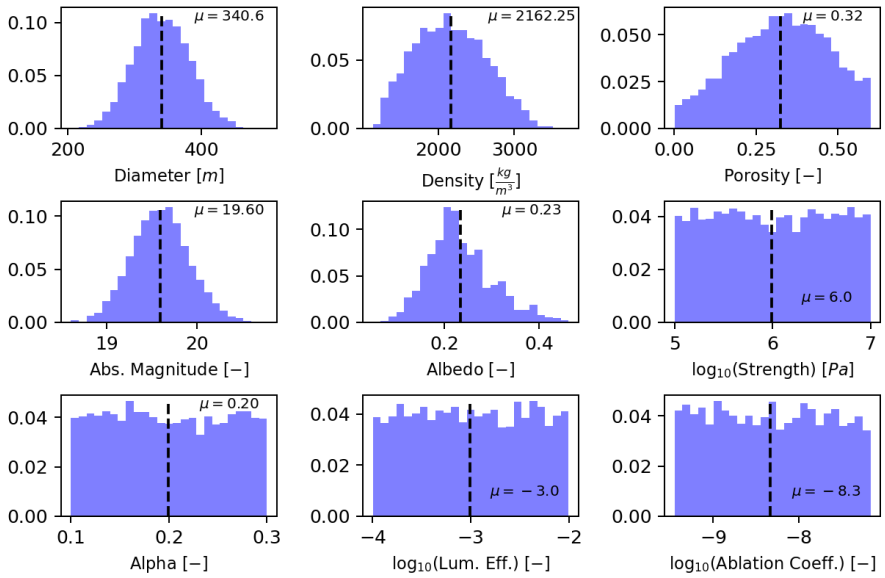

Figure 1. Apophis property distributions used in this study shown as relative probabilities.

A parent population of plausible NEAs with an absolute magnitude similar to that of Apophis was generated. Albedos were assigned from the bimodal distribution of albedos reported for NEAs by Mainzer et al. (2011). The diameter for each case was calculated from the absolute magnitude and albedo. A likely taxonomy was assigned based on the albedo and a simple application of Bayes theorem based on the albedo distribution for each taxonomy and the distribution of asteroids among the taxonomies. A base density appropriate for the taxonomy was generated from the corresponding meteorite density distributions. The base densities were modified by a broad porosity distribution as presented by Mathias et al. (2017) to generate bulk densities. The initial aerodynamic strength, strength scaling factor (Alpha), ablation parameter, and luminous efficiency were all sampled from the distributions as explained in Mathias et al. (2017). From this parent population a set of virtual asteroids were chosen whose parameters matched available characterization measurements of Apophis. An effective diameter of 340 ± 40m was selected based on the radar results of Brozović et al. (2018). Base densities appropriate to Sq taxonomy (Binzel et al., 2009) and LL chondrites (Reddy et al., 2018) were also chosen. The resulting property distributions are shown in Figure 1.

2.3 Nuclear Deflection Mission

The magnitude and direction of the impulse imparted to the asteroid by a given NED can be controlled by adjusting the detonation location relative to the asteroid. Even though it is possible to detonate the NED during a close flyby, rendezvousing with the asteroid allows for a more precise detonation and full control over the standoff distance and relative position.

Both, a chemical propulsion- and a solar electric propulsion (SEP) system offer solutions to deliver a sufficiently sized spacecraft of approximately two metric tons in time for deflection. The arrival date at the asteroid is set to approximately two years before impact, i.e., April 2027. This date offers sufficient time for a deflection to move the asteroid before impact while providing adequate time for mission development including

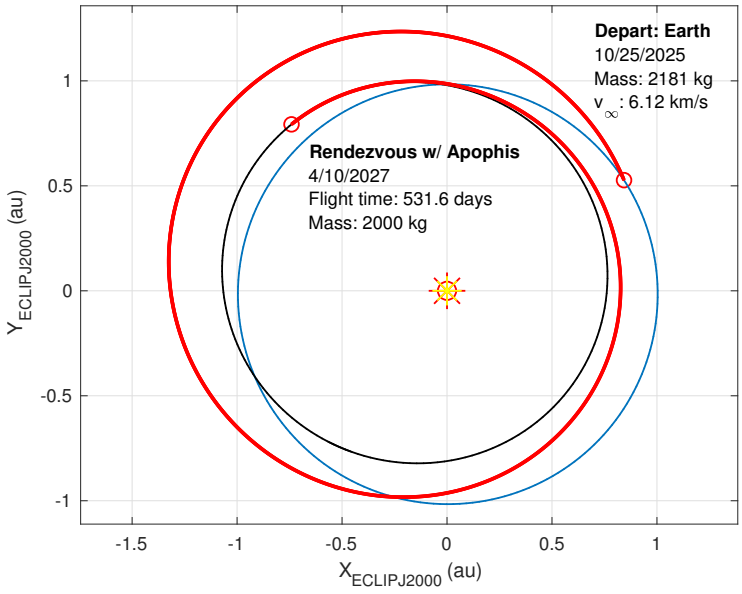

Figure 2. Projection on the ecliptic plane of the rendezvous trajectory using solar electric propulsion. The blue line represents the Earth and the black line represents the asteroid.

a flight time of one and a half years. The Atlas V (531) launcher was adopted as the baseline for the mission.

The most straightforward approach to designing a rendezvous mission is to have the launch vehicle apply an initial impulse to depart from Earth and then apply a second impulsive maneuver at arrival to cancel the hyperbolic excess velocity. The optimal bi-impulsive transfer—the transfer that maximizes the rendezvous mass—leaves Earth on October 31, 2025, with an escape excess specific energy of $C_3 = 5.2$ km^2/s^2 at departure and arrives at the asteroid on March 30, 2027. Atlas V (531) can deliver 4470 kg into the transfer orbit. The hyperbolic excess velocity at arrival is 3.0 km/s. Assuming a specific impulse of 320 s for bi-propellant, the arrival mass at the asteroid is 1720 kg.

Providing the spacecraft with (SEP) instead of chemical propulsion can substantially increase the overall efficiency of the transfer. In this alternative design, the spacecraft mounts two thrusters comparable in performance to the XIPS-25 cm ion thrusters operating at 90 % duty cycle. The power delivered by the solar arrays at 1 AU is 9 kW. The minimum and maximum engine power are 0.4 and 5.1 kW, respectively. The arrival mass is constrained to 2000 kg, and the trajectory is optimized to minimize the departure mass. The optimal solution departs Earth on October 25, 2025, and arrives at the asteroid on April 10, 2027. The departure and arrival dates are similar to the impulsive solution. However, the continuous low-thrust provided by SEP reduces substantially the propellant mass required to cancel the hyperbolic excess velocity at arrival. Furthermore, reducing the propellant mass reduces the overall spacecraft mass, allowing the launcher to deliver the spacecraft into a higher energy orbit. The departure C_3 of the optimal solution is 37.4 km^2/s^2 and the launch mass is 2180 kg. Only 180 kg of propellant is required to rendezvous with the asteroid.

We select the SEP solution as the nominal rendezvous mission because it is significantly more efficient in terms of propellant consumption. Figure 2 depicts the selected rendezvous trajectory.

2.4 Deflection

We investigated the possibility of asteroid disruption by a deflection mission and we focused on the NED deflection technology. It was assumed that the NED produces a yield of $Y_{kt} = 400$ kilotons TNT-equivalent and is detonated at a standoff distance of 100 m. These values were selected such that the deflection impulse in conjunction with Apophis' physical properties only produces weak disruption of the asteroid samples. The weak disruption regime is of most interest for the purposes of this study because it is expected that disruption has the largest effect on risk in this regime. It should be noted that the yield and standoff parameters are non-optimal, but reasonable for NED missions (Sanchez et al., 2009; Bruck Syal et al., 2013; NASA, 2006). The impulse acted in the orbital velocity direction of the asteroid as this is a general, efficient deflection solution (Carusi et al., 2002; Kahle et al., 2006). To estimate the ΔV imparted on the asteroid by the NED, we adopted a semi-empirical relationship based on hydrocode simulations presented in Barbee et al. (2019):

$$A_1 = \sqrt{\frac{Y_{kt} D d^2}{D + 2d}} \tag{1}$$

$$A_2 = \sqrt{1 - \frac{\sqrt{\left(1 + \frac{2d}{D}\right)^2 - 1}}{1 + \frac{2d}{D}}} \tag{2}$$

$$A_3 = \sqrt{\frac{D}{d}\left(1 + \ln\left[\frac{Y_{kt}}{(3.16e-4)d^2}\right]\right) - \left(1 + \frac{D}{d}\right)\ln\left[1 + \frac{D}{d}\right]} \tag{3}$$

$$\Delta V = \frac{16}{\rho}\frac{5750}{D} A_1 A_2 A_3 \tag{4}$$

where Y_{kt} is the yield in kt TNT-equivalent of the NED, d is the NED's standoff distance from the asteroid's surface, D is the asteroid diameter, and ρ is the asteroid's density.

2.5 Disruption

Not all deflection missions are expected to disrupt a target asteroid. Section 2.5.1 presents a physics-based condition that was used to decide if a sample asteroid was disrupted. The fragment sizes are important for subsequent risk analysis as impact consequences vary with impactor size. The fragment size distribution as a result of disruption is described in section 2.5.2.

2.5.1 Disruption Condition

Given a large enough impulse, an asteroid will fragment into multiple pieces. There is a fairly established body of literature that describes this disruption condition for collision processes between asteroids that could also be applied to KI missions (Holsapple & Housen, 2019). The literature is scarcer for NED-induced disruption. In this study, we relied on preliminary findings[5] that suggest weak disruption occurs when the achieved deflection ΔV is larger than 10% of the surface escape velocity v_{esc} of the asteroid[6]:

$$v_{esc} = 2\sqrt{\frac{GM}{D}} \tag{5}$$

where G is the universal gravitational constant and M is the asteroid's mass.

[5] Private communication with Lawrence Livermore Laboratories.

[6] Publications on the matter of NED-induced disruption are anticipated to be forthcoming based on private communications.

2.5.2 Fragmentation Size

The literature suggests to either use a two-segment or a single-segment power law to describe the fragment masses that result from the asteroid's disruption. Large uncertainties for the parameter selection of these power laws still exist. To avoid unnecessary complexity in the face of such uncertainties, a single-segment fragment distribution has been adopted for this work. However, an approach to a two-segment power-law is presented in O'Brien and Greenberg (2005). Here we followed Sanchez et al. (2010) in using the cumulative fragment distribution:

$$N(\geq m) = Cm^{-b} \tag{6}$$

where N is the number of fragments larger than fragment mass fraction m relative to asteroid mass M, and the constants C, b are

$$C = m_{max}^{b} \tag{7}$$

$$b = \frac{1}{1 + m_{max}} \tag{8}$$

In this analysis the cumulative probability distribution provided by Equation (6) was sampled 20 times to generate 20 fragments in the case of disruption. For that purpose, the variable m_{max} provides an upper bound for the sampled fragment mass fractions, while the maximum number of 20 fragments represents a lower bound for the fragment masses. Since the cumulative probability distribution described by Equation (6) was sampled randomly, the actual fragment sizes in each simulation varied within the upper and lower bounds. The upper mass fraction limit m_{max} is generally assumed to be a function of deflection energy as described in Fujiwara et al. (1977). They present the empirical relation

$$m_{max} = 1.66 \times 10^{8} \frac{E_{kin}}{M}^{-1.24} \tag{9}$$

where E_{kin} is the kinetic energy associated with the deflection and the specific deflection energy $\frac{E_{kin}}{M}$ has units of erg/g. Given a constant NED yield as used in the present paper, the excess energy directly depends on the asteroid size/mass. More excess energy is available when a smaller asteroid is disrupted while less—or no—excess energy might be available for a larger one. Given that this study operates at the disruption boundary, little excess energy is generally available leading to only weak disruption. Consequently, few and heavy fragments would be expected in such circumstances. Therefore, and for reasons of comparability between scenarios and to ease interpretation of results, we selected a fairly large, constant upper limit of the fragment size sampling range of $m_{max} = 0.5$. The actual distribution of largest fragment mass fractions realized in one scenario is shown in Figure 3**c**. It is clear that although the upper limit is set to $m_{max} = 0.5$, the sampled values range from 0.13-0.5 with a mean of 0.35. Through random sampling, the effect of a constant fragment size upper limit is somewhat mitigated. Nevertheless, and although the selection of $m_{max} = 0.5$ appears reasonable, this simplifying assumption potentially introduces a bias in the results. Future studies should let the maximum fragment size vary freely with the excess deflection energy.

We assumed that all physical characteristics of the fragments mirror those of the parent body (eg. density, porosity) except for the diameter. As such, the sampled fragment masses directly provide the sizes of the fragments. To conserve mass, it was ensured that the sum of all fragments does not exceed the mass of the parent asteroid. To that end, the 20 sampled fragment masses were successively summed up starting with the largest fragment and moving towards smaller fragment sizes. When the addition of one fragment to the sum exceeded the mass of the parent asteroid, this fragment size was re-calculated such that the summed fragment mass equals the parent asteroid's mass. Figure 3 visualizes the resulting fragment size distributions for the *pure disruption* scenario further explained in section 3.2. Predictably, fragment diameters (plot **a**) are sig-

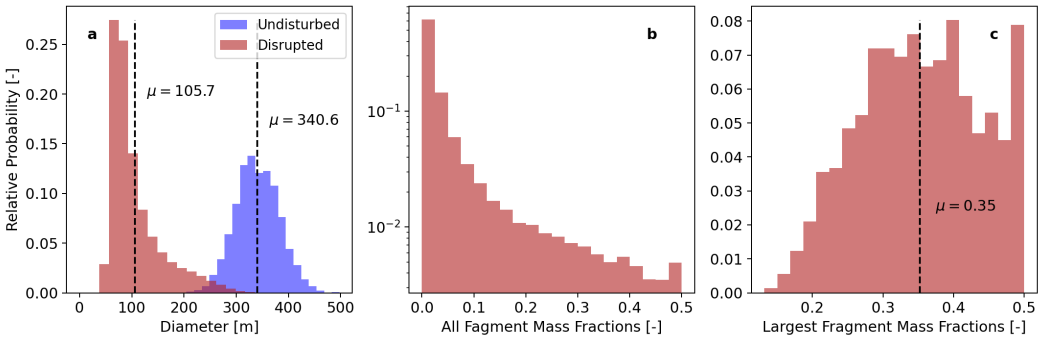

Figure 3. Fragment size plot showing fragment diameters compared to the undisturbed physical property set in (plot **a**), The overall fragment mass fraction distribution of the *pure disruption* case (plot **b**), and the distribution of the largest fragment mass fraction for each disruption (plot **c**). Mass fractions are relative to the parent asteroid mass.

nificantly smaller than those of the parent body. The fragment mass fraction distribution of all generated fragments is shown in plot **b**.

2.5.3 Fragment Dispersion

The fragments that are the result of a disruption event will disperse in largely random directions. However, the overall momentum of the system accounting for the deflection spacecraft and the asteroid will be preserved. This observation provides guidance for a distribution that describes the dispersion of the fragments as presented in Sanchez et al. (2010). The center of mass of the asteroid will have received a velocity change ΔV proportional to the deflection impulse in the direction of the impulse. As such, the mean value of the normal distribution $\mu_{\Delta V}$ that describes the dispersion velocities of the fragments along the impulse direction will be equal to the deflection $\mu_{\Delta V} = \Delta V$. Similarly, the mean value normal to the deflection impulse direction will be zero $\mu_n = 0$. For a normally distributed dispersion model in the three cardinal directions of the Cartesian frame where one axis points along the impulse direction and the other two orthogonal axes are normal to the first axis, the mean vector is

$$\mu_{\mathbf{\Delta V}} = [\Delta V, 0, 0]^T \tag{10}$$

The standard deviation is equal in all three directions and is a function of the overall deflection ΔV as well as the fragment mass mM (Sanchez et al., 2010):

$$\sigma(mM) = \sqrt{\frac{1}{m}}\frac{\Delta V}{k} \tag{11}$$

where k is an empirical value with an appropriate value of $k = 1.4$ according to Sanchez et al. (2010).

2.6 Impact Probability and Risk

Impact probability has been calculated as follows: Assuming a scenario had N virtual asteroids sampled from the orbit solution and K of those impact the Earth, then the impact probability P_I is

$$P_I = \frac{K}{N} \tag{12}$$

In case a disruption occurs, the parent virtual asteroid was counted to impact if at least one of its fragments impacted.

Scenario	P_I [%]	Risk [affected population]	Risk Change [%]
Undeflected	2.70	40 828	baseline case
Pure Disruption	2.57	140 921	+245
Conditional Disruption & ΔV	2.59	123 841	+203
Strong Conditional Disruption & ΔV	2.48	44 913	+10

Table 2. Simulation risk and impact probability (P_I) results for the four case studies.

Risk is the product of the probability that an event occurs and the consequences of that event. For asteroid impact risk assessments, we characterize the risk as the probability of an impact affecting various numbers of people, given range of potential asteroid properties, impact locations, and the overall Earth impact probability. The PAIR model used in this study computes the affected population for each sampled impact case as described in section 2. In the narrow context of this study, we represent the average population risk as the product of impact probability of an Apophis-like scenario and the average estimated affected population. The average risk was calculated by summing up the total casualty count across all Monte Carlo runs and dividing it by the total number of initial asteroids before mitigation. In other words, risk is the average expected damage that accounts for all scenario permutations—samples that miss the Earth, as well as impacts that do and do not cause damage. The average population risk is used as a benchmark metric to compare the hazard level between scenarios.

3 Results

Three main and one minor, fourth case study are discussed in this work. These cases were designed to show how disruption by itself and in conjunction with a weak ΔV by a deflection mission affects risk. The first case study is the *undeflected* scenario where Apophis was allowed to impact without manipulation of the asteroid's state. This scenario establishes the baseline subsequent case studies were compared to. In the second case study, Apophis was always disrupted at the time when the deflection mission would reach it, and the fragments were dispersed randomly, without considering the deflection ΔV. Here, we can assess how *pure disruption* affected impact risk. Although somewhat artificial, since *pure disruption* would not occur in nature, the simulation environment allows us to isolate and compare the effect of disruption on impact risk without complicating aspects such as deflection ΔV. This scenario helps to answer the question of whether a single large impact is more dangerous than multiple small ones, or vice versa. The third case study investigates how the ΔV imparted by the deflection mission changed the situation compared to *pure disruption*. In this case study, the deflected asteroid samples suffered disruption if they met the disruption condition established in section 2.5.1. In such cases, the fragment dispersion included the ΔV imparted to the system. Finally, one additional case study was performed to point out how a strong deflection mission affects impact risk (section 3.4). The parameters of this fourth analysis mirrored those of the previous one with the only difference that the NED deflection mission was 10× stronger (4 Mt instead of 400 kt TNT-equivalent).

Table 2 lists the average population risk and impact probability results for the three case studies. The details of each case study scenario and their results are discussed in the following subsections.

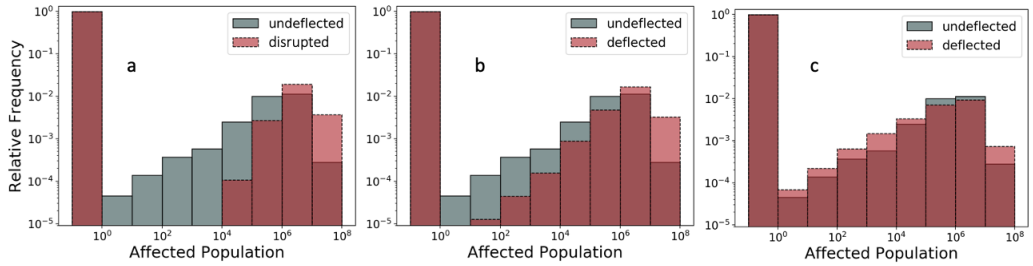

Figure 4. Damage distribution histograms. The grey bars show the damage propensity in terms of affected population for the undeflected scenario in both plots. The overlaid red bars in plot **a** represent the damage of the pure disruption scenario. The red bars in plot **b** show the outcome of the conditional disruption case with overall ΔV. The red bars in plot **c** show the outcome of the conditional disruption case with $10\times$ increased NED yield and therefore stronger ΔV. All zero damage outcomes are represented by the left-most bar.

3.1 Undeflected Risk Scenario

A baseline scenario was generated using 5000 physical property samples and 2648 impact points per corridor. In this undeflected baseline scenario, the impact probability was 2.7 % and the average population risk was 40 828 casualties. For the other scenarios, these baseline figures serve to help interpret how deflection and disruption affect outcomes. The damage distribution of the undeflected case is shown in Figure 4 plot **a** and **b** as grey bars. The overlaid red bars represent the damage distribution of the deflected/disrupted scenarios. The leftmost bar shows those samples that do not cause damage, either because they miss the Earth, or due to an impact in a remote location without casualties. Here the red bar is of similar size as the grey bar behind it because a similar number of scenarios did not yield damage. As should be expected, most often (in $\approx$97 3% of the cases) no damage occurs as reflected by the impact probability. On the other hand, almost every scenario that impacted and involved disruption produced some damage. In fact, only 1 in 15 000 of the impact scenarios that involved disruption did not yield at least some damage.

3.2 Pure Disruption

In the *pure disruption* scenario, the asteroid is disrupted into $N \leq 20$ fragments at the time of deflection as described in section 2.3. The size distribution of the fragments is shown in relation to the undisturbed diameter distribution in Figure 3a. Each fragment received a random dispersion velocity with uniformly distributed random direction (in 3D) and velocity magnitude based on a normal distribution with a standard deviation of 10cm/s. Given that the velocity distributions were zero-mean in direction and magnitude, the overall system trajectory remained unaltered. This range was chosen to provide random impact location separation between fragments after a flight time of two years while providing an upper dispersion bound of about one Earth radius.

Only those virtual asteroids in the orbit solution that are on an Earth-collision course are disrupted. The rationale behind this is based on the observation that a deflection mission could determine if the asteroid is on an Earth-collision trajectory through improved ephemeris as it approaches the asteroid. Only if an asteroid is actually on a collision trajectory would it be deflected and possibly disrupted. Hence, no fragments of virtual asteroids that miss the Earth were generated that could otherwise have been placed on an Earth-impacting trajectory.

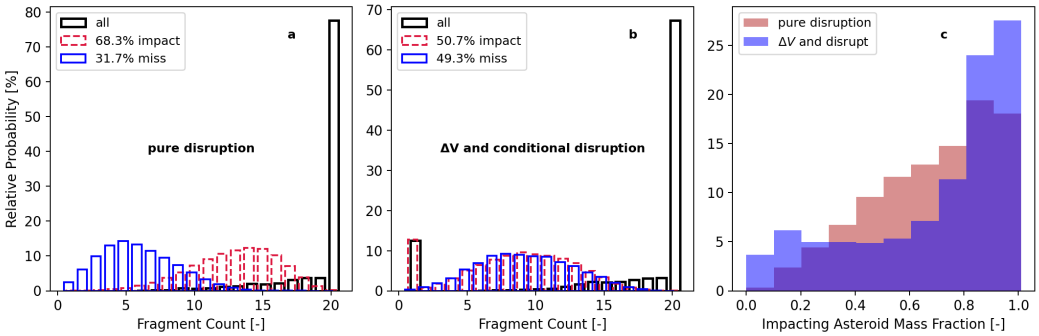

Figure 5. Fragment counts in the *pure disruption* case (plot **a**) and the deflection with conditional disruption case (plot **b**). The deflection reduces the number of impacting fragments. Plot **c** shows the cumulative asteroid mass fraction that still impacts the Earth after disruption for all simulation runs.

Interestingly, the risk in the *pure disruption* case increased dramatically by a factor of 3.45 compared to the unmitigated baseline case. These results indicate that an Apophis-like impact scenario would be significantly worse if it were weakly disrupted into large fragments. Instead of one impact with a singular large body, multiple fragments—still large enough to cause significant damage—hit the Earth in multiple locations. The impact probability remained equal to the *undeflected* scenario. This makes intuitive sense given that the center of mass trajectory of the virtual asteroids was unchanged by random fragment dispersion. Nevertheless, about one third of fragments missed the Earth as a result of disruption (Figure 5**a**).

Figure 4 provides the damage distribution. Two observations can be made: First, while the affected population ranged from 0 to 10^8 in the undeflected scenario, the disrupted scenario produced almost no cases that affected the lower end of the spectrum in the interval $[1, 10^4)$. Only 1 in 8500 cases resulted in damage of <1000 affected people. Second, the maximum-damage, worst-case scenarios became more likely, with an order of magnitude damage likelihood increase for outcomes with 10^7 to 10^8 casualties. To summarize, the disrupted scenario is much less likely to produce a low damage event and much more likely to yield large damage, while maintaining comparable impact probability. The explanation for this observation is that the fragments generated during disruption are large enough to cause significant damage individually and in multiple locations. In the *undisrupted* Apophis impact scenario, impact location is paramount for damage outcome (Rumpf et al., 2016; L. Wheeler et al., 2017) because only a single body hits the Earth. An impact far away from population centers might only yield few casualties. In the *pure disruption* case, on the other hand, several locations are hit—some of which will have low and others high population density. The likelihood of only hitting low damage locations becomes smaller the more fragments hit the surface and appears to be very small with a fragment count upper limit of 20. That is why the low-damage side of the spectrum seems to disappear for the disrupted scenario in Figure 4. The sum of the damages of the individual impacts tends to be greater than the damage caused by a singular Apophis impact. Hence, the maximum damage likelihood also increases as pointed out above.

3.3 Conditional Disruption and ΔV

In the previous scenario (3.2), the asteroid was forced to disrupt into multiple fragments while maintaining the original center of mass trajectory. In this third scenario,

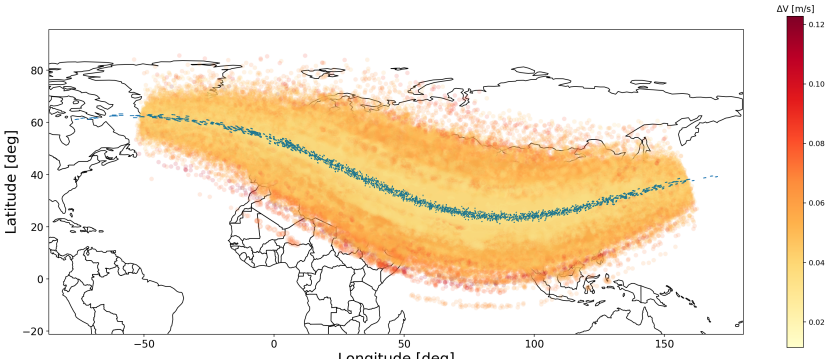

Figure 6. Impact corridor map. The undeflected impact corridor is visualized by a narrow path of blue dots. The impact locations of deflected and possibly disrupted fragments are represented by yellow-to-red color coded markers. The color coding represents the ΔV imparted on the parent virtual asteroid by the NED.

two additional changes were introduced: The first change was that the dispersion velocity of each fragment was now assigned based on the normal distribution described by Equations 10 and 11. In this implementation, the overall deflection impulse ΔV was imparted on the asteroid and its center of mass trajectory will be changed. Figure 6 shows the new impact locations for the samples in this scenario along the original impact corridor. It is clear that the random nature of disruption broadens the potential impact region to a wider swath compared to the originally narrower impact corridor. The overall shape of the corridor is maintained. The color coding of the figure indicates the amount of ΔV received by the parent virtual asteroid. Larger ΔV values shift impact locations farther away from the original impact point until samples are pushed off the Earth. The second change pertains to the disruption itself. While previously, every virtual asteroid was forced to disrupt, in this scenario we applied the disruption condition stating that disruption occurs when $\Delta V \geq 0.1 v_{esc}$ as described in section 2.5.1. For this scenario, this resulted in 87.2 % of the virtual asteroid cases being disrupted and 12.8 % remaining undisrupted.

At first glance, the deflection ΔV had little effect on the scenario outcome producing only small changes in impact probability and risk number in table 2. However, the results indicate positive effects of the mitigation mission compared to the *pure disruption* scenario. While overall risk still increased three-fold due to disruption, the risk increase was 42% less than the *pure disruption* scenario. Just as in the *pure disruption* scenario, the risk increase stems from a larger likelihood to experience worst-case outcomes with casualty numbers between 10^6 and 10^8. In contrast to the *pure disruption* scenario, the deflection mission has the effect of re-introducing the possibility for small scale damage outcomes. Since the center of mass of the virtual asteroids has received a deflection impulse that causes some of them to miss the Earth, the samples' fragments increasingly miss the Earth as well. In other words, with increasing ΔV there is an increasing amount of outcomes in which the asteroid would miss the Earth but a small number of trailing fragments remains on a collision course with the Earth. This behavior is visible in Figure 5 **a** and **b**. Plot **a** represents the fragment count distributions for the *pure disruption* scenario and resolves impacting- as well as Earth-missing fragments. Of all fragments, 31.7 % miss the Earth. With the introduction of a deflection ΔV, as shown in plot **b**, the percentage of Earth-missing fragments increases to 49.3 %. Clearly, the deflection mission pushes more fragments off the Earth. In line with that observation, plot **c** also shows that it is more likely that only a very small mass remains on an Earth-impacting

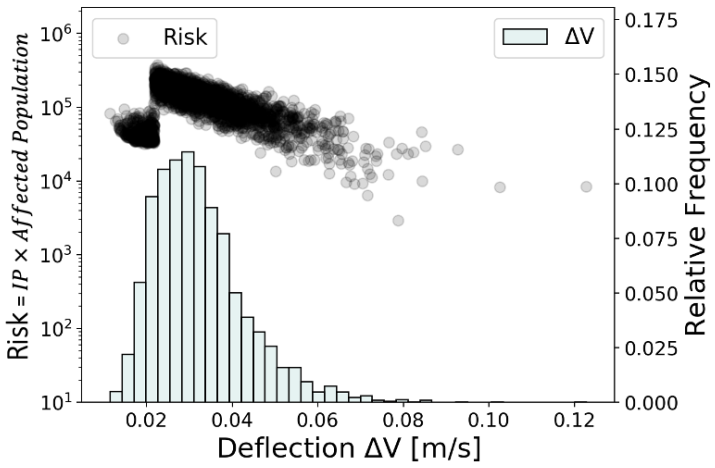

Figure 7. Left hand axis shows risk as a scatter plot over the realized ΔV range for the *deflection with conditional disruption* scenario. The histogram shows the propensity of ΔV values observed in the simulation and its values are plotted against the right-hand axis. Larger ΔV values correspond to increased likelihood of disruption, which is represented by a threshold value here. The sudden risk increase for increasing ΔV values is visible at about $\Delta V = 0.025\,\mathrm{m/s}$ and corresponds to the disruption condition $\Delta V \geq 0.1 v_{esc}$.

trajectory. With a smaller number of fragments and less mass impacting the Earth the likelihood to produce small aggregate casualty outcomes increases again. Figure 4**b** reflects this increase in small damage outcomes, compared to the pure disruption case. Figure 5**c** also shows more events where the full mass impacted the Earth. Because this third scenario applied conditional disruption, about 12.8 % of asteroids remain intact (as opposed to none in the previous scenario). The corresponding spike in single fragment/asteroid impacts is visible as well in plot **b**. The presence of full asteroid impacts explains the increased propensity of large masses impacting the Earth.

As previously pointed out, disruption increases risk significantly in the present analysis and Figure 7 visualizes the increase dynamics on the ΔV spectrum. The figure shows a scatter plot of the risk outcome for each physical property sample. Against the right-hand side, a histogram shows the propensity of corresponding ΔV values. Given that the deflection impulse is constant, smaller ΔV values correspond to more massive objects. A more massive object exhibits a larger escape velocity, which is less likely to disrupt according to the disruption criteria described in section 2.5. The disruption threshold is clearly visible in this figure at $\Delta V = 0.025\,\mathrm{m/s}$. Here, risk shows a sudden increase for larger ΔV values (decreasing mass). Risk levels only reduce to pre-disruption levels at about $\Delta V = 0.07\,\mathrm{m/s}$. In other words, a much larger effort is needed to shift the majority of realized ΔV values into a risk region that offers equivalent risk values as an undisrupted scenario. Even more effort and larger ΔV values are needed to continue robust risk reduction beyond that point. Still, the risk scatter plot shows a general trend of decreasing risk with larger ΔV (stronger deflection missions relative to asteroid size). That means that sufficiently energetic deflection missions (relative to asteroid size) are effective at reducing risk. Future research should investigate the relation between desired ΔV values accomplished by a deflection mission and the resulting risk values. One important take-away from this paper is that the work presented here should be extended to provide guidance for mitigation mission designers as to which deflection impulse is needed to decrease risk to safe levels while allowing for the possibility of disruption.

3.4 Strong Conditional Disruption and ΔV

The point of the fourth case study is to show how a much larger deflection impulse affects the impact risk situation. We used the same parameters as in the case with conditional disruption and ΔV (section 3.3) but simulated a NED deflection mission that was ten times stronger, or 4 Mt instead of 400 kt TNT-equivalent, than previously. The increased deflection energy has the immediate result that impact risk, despite being disrupted, only changes slightly by 10 % compared to the undisrupted case. However, even with a 10× deflection energy change, impact risk still increased (see Table 2). Interestingly, the damage distribution also remained comparable to the undisrupted case as shown in Figure 4**c**. It is not clear why the damage distribution outcome is so similar despite very different dynamics in a disrupted scenario. It is possible that this is an unusual, special outcome of our parameter selection. Impact probability showed a minor reduction from 2.7 % to 2.48 %. The fact that merely one fragment impact in each simulation run is necessary to produce the same impact probability as the undisturbed case explains how this is possible. Despite having received a strong deflection impulse, lingering fragments might still impact the Earth and support an only minor change in impact probability. Overall, this case study demonstrates the effectiveness of deflection missions despite the aggravating circumstances of disruption. Impact risk decreased markedly compared to the *pure disruption* scenario. More work is needed to establish by how much deflection mission effort needs to be increased to produce safe deflection in the face of disruption.

4 Changing Apophis' Size

Disruption is not likely to increase risk for all asteroids. Changes in risk will depend on several factors. As a starting point to investigate this question further, we varied the size of Apophis and evaluated the resulting risk outcomes for the undisrupted as well as the disrupted case. Figure 8 presents the outcome of this effort. Each dot represents a full simulation in which all diameter values have been reduced by the scaling factor marked on the x-axis. The linear relationship between scaling factor and distribution mean diameter is plotted against the left-hand axis. The right hand axis shows risk values for scenarios that are equivalent to the *pure disruption* and the undisrupted cases.

The results show that risk increases exponentially with increasing asteroid size when disruption occurs. Conversely, risk appears to be leveling off for larger asteroids that impact as a monolith[7], supposedly until global effects would increase the risk slope for larger asteroids. Similar behavior has been observed in Rumpf et al. (2017). A likely explanation is that, while the local damage of a singular impact can affect one population center, it is harder to reach other centers that are dispersed around the globe. Multiple fragments can affect multiple population centers independently, which enables exponential risk growth. Interestingly, there are two distinct size regimes. In the first regime a single impactor produces more dangerous impact scenarios for small asteroids. This regime stops at a point where the risk outcome is equivalent for disrupted and undisrupted (single impactor) asteroids. Beyond that point, the fragmented scenarios rapidly produce more dangerous impact scenarios. In this analysis, the critical scaling factor that yielded equivalent risk outcomes was 0.63 (corresponds to a mean diameter of $D = 214$ m) although it should be expected that this value varies for other scenarios. As such, the results presented in this paper only reflect risk outcomes for large asteroid impact scenarios comparable in size to Apophis. Future research should investigate the relationship between physical properties and how they affect risk changes considering disruption. Such

[7] The detailed reasons for this dynamic should be the subject of future investigations. Similar behaviour has already been observed in Rumpf et al. (2017).

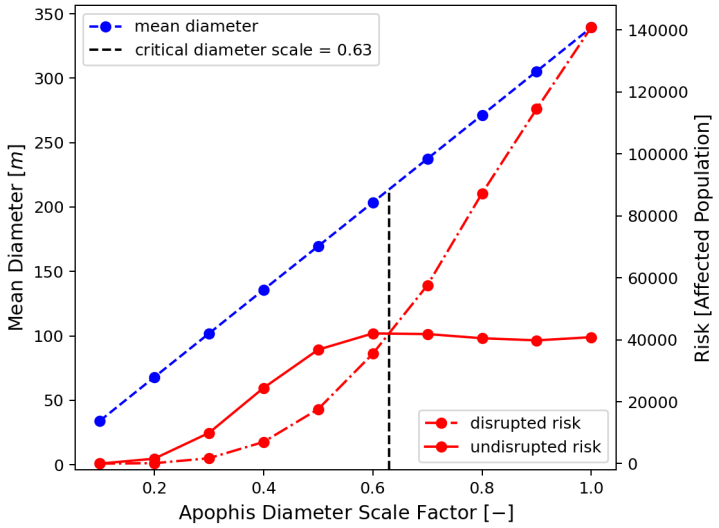

Figure 8. Risk response to Apophis diameter scaling in the *pure disruption* scenario. The blue dashed line shows the mean diameter corresponding to the diameter scaling value while the red dashed-dotted line shows risk for each diameter scaling value. The red solid line shows the baseline risk of the undisrupted scenario.

analysis should also estimate varying upper limits for the maximum fragment sizes and fragment piece counts depending on physical properties and excess deflection energy.

5 Double Counting of Casualties

The simulation tools employed in this analysis could not compensate for the potential issue of casualty double counting when an asteroid yielded multiple fragments that impact the Earth. This issue would be a problem if the impact locations of fragments were close enough to each other such that their damage regions overlap. In such a case, our results would suffer from double counting of casualties in the overlapping damage region, which would lead us to overestimate casualty numbers.

It was possible to gain insight into this concern because the output files record the impact latitude and longitude of each fragment along with their damage radius on the surface of the Earth. The following analysis only considers those fragments that actually hit the Earth and does not include those that fly past the Earth. We calculated the extent and location of each damage region by each fragment (of one parent asteroid) on the Earth and analysed them for overlaps. The damage area overlap ratio ($DAOR$) is defined as the fraction of overlapping damage area between all fragments relative to total damage area of all fragments.

$$DAOR = \frac{\sum_{i=1}^{N=20} \sum_{j=i+1}^{N=20} A_{overlap,i,j}}{\sum_{i=1}^{N=20} A_{Damage,i}} \tag{13}$$

where $A_{overlap,i,j}$ is the damage area overlap between fragment i and j, and $A_{Damage,i}$ is the damage area of fragment i. Equation (13) reflects the fact that only impacting fragments are considered to calculate overlap ratios and those samples and fragments that miss the Earth do not enter that calculation. Figure 9 shows the outcome of that analysis.

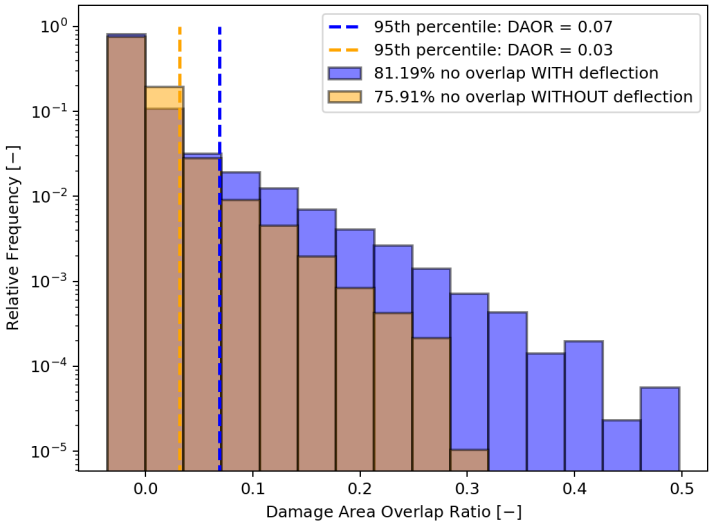

Figure 9. Damage area overlap ratios that were observed in the *pure disruption* case study and the scenario with deflection and conditional disruption. In the vast majority of cases no overlap in damage area was detected and thus casualty damage counting is deemed to have a minimal effect on results.

In the large majority of cases no overlap between fragment damage regions was detected (75.9 % for *pure disruption*, and 81.2 % with deflection). This indicates that the separation between fragment impact locations was usually far enough to ensure no overlap of damage regions. In those instances when overlap was recorded, the overlap amount tended to be small. In the *pure disruption* scenarios, 95 % of cases showed an overlap of less than 3 % of total damage area. The completely random dispersion of fragments in this scenario explains the small overlap number. On the other hand, dispersion was more directed in the scenarios with applied ΔV. But even in these cases, only about 1 in 1000 scenarios showed overlaps of up to 30 % while the large majority showed no overlap. The average overlap was only 0.97 %. While the general outcome is that overlap areas were very small, double counting of affected population has likely occurred in rare cases. However, it is unlikely that double counting skewed the results significantly relative to the overall change in risk as a result of disruption ($> 3\times$ risk increase). This analysis implies that double counting of affected population did not have a significant effect on the conclusions of this paper.

6 Conclusions and Future Work

Asteroid Apophis served as the basis to estimate how disruption by a deflection mission could affect impact risk compared to an undisrupted scenario. An archival orbit solution from 2004 with a 2.7 % impact probability in 2029 provided the corresponding impact corridor and impact locations. This analysis shows that disruption can increase impact risk by more than a factor of three for the two main case studies compared to an unaltered Apophis impact scenario. A fourth case study provided a short glimpse at the effectiveness of a more powerful NED deflection mission.

The first case study disrupted the asteroid at the time of deflection mission arrival—two years before impact—without imparting a deflection ΔV. Risk increased by a factor of 3.45 highlighting the concern that disruption could be of major importance to mitigation mission planners to avoid unintentional aggravation of the threat situation.

The second case study imparted the intended deflection ΔV and conditionally disrupted the asteroid samples based on physical considerations. The deflection mission succeeded in reducing impact risk compared to the *pure disruption* scenario but still yielded a three-fold risk increase compared to the undeflected scenario. This outcome indicates that mitigation missions have the desired effect of reducing impact risk but the possibility of disruption might need to be considered when sizing the spacecraft

The analysis makes it clear that a disrupted asteroid can be much more dangerous than an undisrupted one. The reason is that, in this scenario, multiple fragment impacts in several locations are worse than one large impact in a single location. In a disruption event with multiple impacts the damage of all fragments are summed up ensuring that low-damage outcomes became unlikely and large damage outcomes became significantly more likely.

However, the blanket statement that disruption always yields larger impact risk is wrong. Additional analysis investigated the dependency of asteroid size to impact risk. While large asteroids, such as Apophis, show increased impact risk after disruption, a crossover size exists below which smaller asteroids show less impact risk after disruption. This observation should serve as motivation to further investigate the dependency of disruption and post-disruption impact risk to physical properties. Such work could yield science targets for future exploration missions with the aim of characterising those characteristics that drive disruption.

It should be noted that we used several simplifying assumptions in this study. The upper limits for fragment count and fragment relative size were set to 20 and 0.5, respectively. Future analysis should let these parameters vary freely or investigate their effect on results. Although within the range of realistic values, the deflection mission parameters in terms of yield and stand-off detonation distance were set constant and should be considered non-optimal. Finally, in those scenarios where a deflection ΔV was imparted, the direction of the deflection was constant and accelerated the asteroid. In a real mission, a NED deflection mission could adjust the deflection direction under optimality considerations.

The work presented here should be extended to investigate the dependency of disruption and post-disruption impact risk on changes in NED yield (or stand-off distance at which it is detonated). Larger NED yields will produce stronger disruption which is beneficial for risk reduction in two ways. First, the fragments are dispersed more forcefully which will cause more of them to miss the Earth and the fragments themselves should be smaller, which produces less damage should they impact. Second, the imparted ΔV produces a bias that shifts the deflected asteroid and its fragments off the Earth. In concert these two effects should produce lower impact risk with increasing NED yield. This expectation was further demonstrated in the fourth case study where a $10\times$ stronger NED deflection mission was employed compared to the other case studies. The effect was a marked decrease in impact risk. However, significant impact risk remained even in this scenario. Future work should identify desired NED yields to robustly deflect asteroids considering the possibility of disruption. The question to what extent the selection of the upper limits for fragment count and maximum fragment mass introduces bias in results should also be addressed as part of such analysis.

Finally, the understanding of NED interactions with asteroids for the purpose of asteroid deflection would benefit from more thorough investigation. Well-documented work is needed to robustly estimate achievable ΔV values given a NED yield and target asteroid properties. In addition, the disruption behavior of asteroids due to a NED explosion is uncertain. Analysis such as presented here would greatly improve with better models for the interaction of NEDs with asteroids.

Acknowledgments

This work has been funded in large part by NASA's Planetary Defense Coordination Office (PDCO). Resources supporting this work were provided by the NASA High-End Computing (HEC) Program through the NASA Advanced Supercomputing (NAS) Division at Ames Research Center. Part of this research was conducted at the Jet Propulsion Laboratory, California Institute of Technology, under a contract with NASA. Michael Aftosmis and Darrel Robertson significantly improved the quality of this paper through their thoughtful internal reviews. The authors would like to thank Donovan Mathias, and Brent Barbee for thoughtful discussions that helped improve the quality of this work. Datasets for this research are available in this in-text data citation reference: Rumpf (2021).

References

Aftosmis, M. J., Mathias, D. L., & Tarano, A. M. (2019). Simulation-based height of burst map for asteroid airburst damage prediction. *Acta Astronautica*, *156*(November 2017), 278–283. Retrieved from `https://doi.org/10.1016/j.actaastro.2017.12.021` doi: 10.1016/j.actaastro.2017.12.021

Alvarez, L. W., Alvarez, W., Asaro, F., & Michel, H. V. (1980). Extraterrestrial cause for the cretaceous-tertiary extinction. *Science*, *208*(4448), 1095–1108. Retrieved from `http://www.sciencemag.org/content/208/4448/1095` doi: 10.1126/science.208.4448.1095

Barbee, B. W., Sarli, B. V., Lyzhoft, J., Chodas, P. W., & Englander, J. A. (2019). Spacecraft Mission Design for The Mitigation of The 2019 PDC Hypothetical Asteroid Threat. In *Iaa planetery defence conference* (Vol. 1, pp. 1–15). Retrieved from `https://ntrs.nasa.gov/archive/nasa/casi.ntrs.nasa.gov/20170004646.pdf`

Binzel, R. P., Rivkin, A. S., Thomas, C. A., Vernazza, P., Burbine, T. H., DeMeo, F. E., ... Birlan, M. (2009, April). Spectral properties and composition of potentially hazardous Asteroid (99942) Apophis. *Icarus*, *200*(2), 480-485. doi: 10.1016/j.icarus.2008.11.028

Brozović, M., Benner, L. A. M., McMichael, J. G., Giorgini, J. D., Pravec, P., Scheirich, P., ... Lawrence, K. J. (2018, January). Goldstone and Arecibo radar observations of (99942) Apophis in 2012-2013. *icarus*, *300*, 115-128. doi: 10.1016/j.icarus.2017.08.032

Bruck Syal, M., Dearborn, D. S., & Schultz, P. H. (2013, sep). Limits on the use of nuclear explosives for asteroid deflection. *Acta Astronautica*, *90*(1), 103–111. Retrieved from `http://linkinghub.elsevier.com/retrieve/pii/S0094576512004031` doi: 10.1016/j.actaastro.2012.10.025

Carusi, A., Valsecchi, G. B., D'Abramo, G., & Boattini, A. (2002). Deflecting neos in route of collision with the earth. *Icarus*, *159*(2), 417–422. doi: 10.1006/icar.2002.6906

Chapman, C. R., & Morrison, D. (1994). Impacts on the Earth by asteroids and comets: assessing the hazard. *Nature*, *367*(January). Retrieved from `http://www.nature.com/nature/journal/v367/n6458/abs/367033a0.html`

Cheng, A. F., Rivkin, A. S., Michel, P., Atchison, J., Barnouin, O., Benner, L., ... Thomas, C. (2018). AIDA DART asteroid deflection test: Planetary defense and science objectives. *Planetary and Space Science*, *157*. doi: 10.1016/j.pss.2018.02.015

Chesley, S. R. (2006, January). Potential impact detection for near-earth asteroids: the case of 99942 apophis (2004 mn 4). In D. Lazzaro, S. Ferraz-Mello, & J. A. Fernández (Eds.), *Asteroids, comets, meteors* (Vol. 229, p. 215-228). doi: 10.1017/S1743921305006769

Chyba, C. F., Thomas, P. J., & Zahnle, K. J. (1993). The 1908 Tunguska explosion: atmospheric disruption of a stony asteroid. *Nature*, *361*(January). Retrieved from `http://www.nature.com/nature/journal/v361/n6407/pdf/`

361040a0.pdf

Covey, C., Thompson, S. L., Weissman, P. R., & MacCracken, M. C. (1994). Global climatic effects of atmospheric dust from an asteroid or comet impact on Earth. *Global and Planetary Change*, *9*(3-4), 263–273. doi: 10.1016/0921-8181(94)90020-5

Fujiwara, A., Kamimoto, G., & Tsukamoto, A. (1977). Destruction of basaltic bodies by high-velocity impact. *Icarus*, *31*(2), 277–288. doi: 10.1016/0019-1035(77)90038-0

Hergarten, S., & Kenkmann, T. (2015). The number of impact craters on Earth: Any room for further discoveries? *Earth and Planetary Science Letters*, *425*, 187–192. Retrieved from http://dx.doi.org/10.1016/j.epsl.2015.06.009 doi: 10.1016/j.epsl.2015.06.009

Holsapple, K. A., & Housen, K. R. (2019). The catastrophic disruptions of asteroids: History, features, new constraints and interpretations. *Planetary and Space Science*, *179*(August), 104724. Retrieved from https://doi.org/10.1016/j.pss.2019.104724 doi: 10.1016/j.pss.2019.104724

Kahle, R., Hahn, G., & Kührt, E. (2006, jun). Optimal deflection of NEOs en route of collision with the Earth. *Icarus*, *182*(2), 482–488. Retrieved from http://linkinghub.elsevier.com/retrieve/pii/S0019103506000339 doi: 10.1016/j.icarus.2006.01.005

Mainzer, A., Grav, T., Bauer, J., Masiero, J., McMillan, R. S., Cutri, R. M., ... Wasserman, L. H. (2011, December). NEOWISE Observations of Near-Earth Objects: Preliminary Results. *The Astronomical Journal*, *743*(2), 156. doi: 10.1088/0004-637X/743/2/156

Mathias, D. L., Wheeler, L. F., & Dotson, J. L. (2017). A Probabilistic Asteroid Impact Risk Model: Assessment of Sub-300 m Impacts. *Icarus*, *289*, 106–119. Retrieved from http://linkinghub.elsevier.com/retrieve/pii/S0019103516307126 doi: 10.1016/j.icarus.2017.02.009

NASA. (2006). *2006 Near-Earth Object Survey and Deflection Study* (Tech. Rep. No. December). Author.

O'Brien, D. P., & Greenberg, R. (2005). The collisional and dynamical evolution of the main-belt and NEA size distributions. *Icarus*, *178*(1), 179–212. doi: 10.1016/j.icarus.2005.04.001

Popova, O. P., Jenniskens, P., Emelyanenko, V., Kartashova, A., Biryukov, E., Khaibrakhmanov, S., ... Mikouchi, T. (2013, nov). Chelyabinsk airburst, damage assessment, meteorite recovery, and characterization. *Science (New York, N.Y.)*, *342*(6162), 1069–73. Retrieved from http://www.ncbi.nlm.nih.gov/pubmed/24200813 doi: 10.1126/science.1242642

Pravec, P., Vokrouhlický, D., Polishook, D., Scheeres, D. J., Harris, A. W., Galád, A., ... Leroy, A. (2010). Formation of asteroid pairs by rotational fission. *Nature*, *466*(7310), 1085–1088. doi: 10.1038/nature09315

Reddy, V., Sanchez, J. A., Furfaro, R., Binzel, R. P., Burbine, T. H., Le Corre, L., ... Brozovic, M. (2018, March). Surface Composition of (99942) Apophis. *The astronomical journal*, *155*(3), 140. doi: 10.3847/1538-3881/aaaa1c

Reinhardt, J. C., Chen, X., Liu, W., Manchev, P., & Paté-Cornell, M. E. (2016). Asteroid Risk Assessment: A Probabilistic Approach. *Risk Analysis*, *36*(2), 244–261. doi: 10.1111/risa.12453

Robertson, D. K., & Mathias, D. L. (2019). Hydrocode simulations of asteroid airbursts and constraints for Tunguska. *Icarus*, *327*(October 2018), 36–47. doi: 10.1016/j.icarus.2018.10.017

Rumpf, C. M. (2021). *Data Set: Asteroid Impact Risk Changes Due To Disruption By A Deflection Mission.* Mendeley Data. doi: 10.17632/59jr28jc5d.2

Rumpf, C. M., Lewis, H. G., & Atkinson, P. M. (2016). On the influence of impact effect modelling for global asteroid impact risk distribution. *Acta Astronautica*, *123*, 165–170. Retrieved from http://linkinghub.elsevier.com/retrieve/

pii/S0094576515302988 doi: 10.1016/j.actaastro.2016.03.015

Rumpf, C. M., Lewis, H. G., & Atkinson, P. M. (2017). Asteroid impact effects and their immediate hazards for human populations. *Geophysical Research Letters*, *44*(8), 3433–3440. doi: 10.1002/2017GL073191

Rumpf, C. M., Mathias, D. L., Wheeler, L., Dotson, J., Barbee, B. W., Roa, J., ... Farnocchia, D. (2020). Deflection driven evolution of asteroid impact risk under large uncertainties. *Acta Astronautica*, *176*(June), 276–286. Retrieved from https://doi.org/10.1016/j.actaastro.2020.05.026 doi: 10.1016/j.actaastro.2020.05.026

Sanchez, J. P., Colombo, C., Vasile, M., & Radice, G. (2009). Multicriteria comparison among several mitigation strategies for dangerous near-Earth objects. *Journal of Guidance, Control, and Dynamics*, *32*(1), 121–142. doi: 10.2514/1.36774

Sanchez, J. P., Vasile, M., & Radice, G. (2010). Consequences of asteroid fragmentation during impact hazard mitigation. *Journal of Guidance, Control, and Dynamics*, *33*(1), 126–146. doi: 10.2514/1.43868

Sánchez, P., & Scheeres, D. J. (2014). The strength of regolith and rubble pile asteroids. *Meteoritics and Planetary Science*, *49*(5), 788–811. doi: 10.1111/maps.12293

Seidelmann, P. K. (1977, October). Numerical values of the constants of the Joint Report of the Working Groups of IAU Commission 4. *Celestial Mechanics*, *16*(2), 165-177.

Shapiro, I. I., Vilas, F., A'Hearn, M., Cheng, A. F., Abell, P., Benner, L. A., ... Jackson, P. (2010). *Defending Planet Earth : Near-Earth Object Surveys and Hazard Mitigation Strategies* (Tech. Rep.). Washington D.C.: National Research Council.

Stokes, G. H., Barbee, B. W., Bottke, W. F., Buie, M. W., Chesley, S. R., Chodas, P. W., ... Yeomans, D. K. (2017). *Update to Determine the Feasibility of Enhancing the Search and Characterization of NEOs* (Tech. Rep.). National Aeronautics and Space Administration. Retrieved from https://cneos.jpl.nasa.gov/doc/2017_neo_sdt_final_e-version.pdf

Vokrouhlický, D., Farnocchia, D., Čapek, D., Chesley, S. R., Pravec, P., Scheirich, P., & Müller, T. G. (2015, May). The Yarkovsky effect for 99942 Apophis. *icarus*, *252*, 277-283. doi: 10.1016/j.icarus.2015.01.011

Walsh, K. J., Richardson, D. C., & Michel, P. (2008). Rotational breakup as the origin of small binary asteroids. *Nature*, *454*(7201), 188–191. doi: 10.1038/nature07078

Wheeler, L., Mathias, D., & Dotson, J. (2017). Sensitivity of Impact Risk to Uncertainty in Asteroid Properties and Entry Parameters. In *Annual division of planetary sciences meeting.* Provo, UT: American Astronomical Society. Retrieved from https://ntrs.nasa.gov/citations/20180007149

Wheeler, L. F., Register, P. J., & Mathias, D. L. (2017). A fragment-cloud model for asteroid breakup and atmospheric energy deposition. *Icarus*, *0*, 149–169. Retrieved from http://linkinghub.elsevier.com/retrieve/pii/S0019103516307989 doi: 10.1016/j.icarus.2017.02.011